ARTICLE

OPEN

Check for updates

Atmospheric rivers that make landfall in India are associated with flooding

Shanti Shwarup Mahto [1], Munir Ahmad Nayak [2], Dennis P. Lettenmaier[3] & Vimal Mishra [1,4 ✉]

Atmospheric rivers often cause extreme precipitation at landfall, leading to floods. However, the underlying physical mechanism of atmospheric rivers and their linkage with flooding in India remain unrecognized. Here we use reanalysis and observations to diagnose the drivers of atmospheric rivers and unravel their crucial role in extreme precipitation and floods during 1951–2020. Moisture transport has significantly increased during 1951–2020, which is associated with strengthening winds that transport water vapor from the oceans. However, while there is a suggestive corresponding increase in the frequency of atmospheric rivers, it is not statistically significant. The atmospheric river catalogue that we developed shows that about 65% of landfalling atmospheric river were linked to floods during the 1985–2020 period. In addition, seven of India's ten most severe floods in the summer monsoon season with substantial mortality were associated with atmospheric rivers. Better understanding and prediction of atmospheric rivers is crucial for flood mitigation.

[1] Earth Sciences, Indian Institute of Technology (IIT) Gandhinagar, Gandhinagar, India. [2] Civil Engineering, National Institute of Technology (NIT) Srinagar, Srinagar, India. [3] Department of Geography, University of California, Los Angeles, CA, USA. [4] Civil Engineering, Indian Institute of Technology (IIT) Gandhinagar, Gandhinagar, India. ✉email: vmishra@iitgn.ac.in

The summer monsoon season brings copious rainfall to India, resulting from moisture-laden winds that reach the subcontinent and originate near the equator[1]. Extreme precipitation events in the region occur almost exclusively during the summer monsoon, albeit with substantial interannual and intraseasonal variability[2–4]. Daily and sub-daily precipitation extremes have increased in recent decades and are likely to rise as the climate continues to warm[5,6]. India experiences floods mainly caused by extreme precipitation, which result in annual economic losses that average about USD 3 billion annually[7]. Some extreme precipitation events can be attributed to the landfalling atmospheric rivers (ARs), defined as long and narrow corridors of strong horizontal water vapor transport[8]. Extreme precipitation caused by ARs often triggers large floods over the coastal western United States[8,9]. ARs have emerged as the dominant source of moisture transport in several regions across the globe[10–16], a list to which we show the Indian subcontinent can now be added.

Atmospheric rivers can be classified based on the magnitude of their moisture transport and impacts on the land surface[17]. Atmospheric pressure gradients and moisture availability allow ARs to persist for periods as long as a week[17,18]. The magnitude of ARs increases with their duration, related to the size of the moisture uptake region over oceans[17]. For instance, long-duration ARs that affect the Western U.S. have a moisture uptake region that includes most of the northern Pacific Ocean[10]. Increased frequency and intensity of ARs have been observed in many areas across the globe[10] and are expected to increase further in a warmer world[18,19]. However, changes in ARs in the south Asian monsoon region have remained unrecognized primarily due to strong seasonality in precipitation and synoptic scale monsoonal flow[10,16,18]. Therefore, identifying the drivers of monsoon season, ARs deserves a separate investigation[20]. The south Asian monsoon system is projected to transport more moisture under a warming climate[3,10,21], which may lead to an increased frequency of ARs making landfall over India.

Notwithstanding the prominent role of ARs in extreme precipitation and flooding and their benefits for water supply[17], the characteristics and driving mechanisms of ARs in India remain largely unrecognized[22,23]. Moreover, flooding due to multiday extreme precipitation has substantially increased in India in the recent past[3,4,6], which is projected to increase further in the future[24]. Here, we use high-resolution atmospheric fields from the European Reanalysis Version 5 (ERA5)[25] along with observed precipitation from the India Meteorological Department (IMD)[26], and a historical flood database from Dartmouth Flood Observatory, the University of Colorado, USA (https://floodobservatory.colorado.edu/Archives/index.html) to examine the occurrence of ARs and their linkage with major floods in India over the last 70 years.

Results and discussion

Observed changes in atmospheric rivers. We identified ARs using the methodology developed in the previous studies[20,27], which is applied to daily Vertically Integrated Vapor Transport (IVT) exceeding the 85th percentile (on an ERA5 grid cell basis) to perform a preliminary identification of clusters forming ARs. Dimensional criteria (length, width, circularity) were then applied to obtain a final set of ARs (Fig. S1, see methods for details). On this basis, we found that India experienced 596 major AR events from 1951–2020, totaling 1520 AR days. More than 95% (574 AR events or 1497 AR days) of these ARs occurred during the summer monsoon season (June-September). We focused only on those ARs that occurred in the summer monsoon season, as only about 4% of total ARs by number (and 3% of AR days) happened during the non-monsoon season during the 1951–2020 period.

During the summer monsoon, ARs occur about 28% of the days in July, followed by August (22%), June (15%), and September (6%) [Fig. S1a]. Strong seasonality in moisture transport prevails over all parts of India, which accounts for the dominance of the summer monsoon in the AR statistics. For instance, vertically integrated vapor transport (IVT) is low (~150 kg m^{-1} s^{-1}) during January-May, but rapidly increases during the monsoon season to an average of ~350 kg m^{-1} s^{-1}. IVT declines (to an average of less than 200 kg m^{-1} s^{-1}) during the post-monsoon season (Fig. S1b). Area average mean IVT is anomalously high (greater than 500 kg m^{-1} s^{-1}) during the summer monsoon season period over the Arabian Sea, Bay of Bengal, and parts of the Indian land mass (Fig. S2).

Our analysis indicates that AR-related moisture transport over India has a considerable spatial variability (see also ref.[23]). In particular, the eastern part of the Indo-Gangetic plain and peninsular India experience higher IVT (>500 kg m^{-1} s^{-1}) than the other regions (Fig. S3). Consistent with relatively higher IVT, the frequency of occurrence of ARs is also higher in the lower Indo-Gangetic plain and peninsular India during the summer monsoon season (Fig. S1c). ARs affect peninsular India during the summer monsoon season, while northern India experiences ARs mainly in July and August (Fig. S4).

We find a moderately increasing trend but not significant in the frequency of ARs in the summer monsoon season during 1951–2020 (Fig. 1a). On the other hand, the mean IVT anomaly (40-120E, 10S-25N) in the summer monsoon season has significantly (p-value = 0.0001) increased (Fig. 1b). The increase in IVT during the summer monsoon season can be partly associated with the warming climate that accelerates anomalous moisture uptake[10], leading to the rising trend in the frequency of ARs[19,28]. Our results show that the parts of the Arabian Sea, northern India, and peninsular India experienced a significant increase in the AR frequency during the summer monsoon season (Fig. 1c). We hypothesize that this increase in AR frequency results in the observed rise in extreme precipitation over India[7,23,29,30], which in turn has caused increased flooding[31,32]. A similar link has been reported for other regions[10,17,19,33,34]. However, this linkage between ARs and flooding in India has been unrecognized.

Out of the top 1/3rd (~190 out of 574) AR events, 54% occurred in the most recent three decades (1991–2020) [Fig. S12], with a severity 10% higher than the average severity score of all ARs. Therefore, the frequency and severity of ARs show an increasing trend in India in recent decades. We provide the list of ARs, which displays a decreasing order of severity (see AR catalog, Supplemental Data 1). Both the maximum and mean IVT of ARs over land have also increased significantly (p < 0.05) over the period 1951–2020 at a rate of ~1 kg m^{-1} s^{-1} and 0.3 kg m^{-1} s^{-1} per year, respectively (Fig. S5), with the most prominent increase over the Indo-Gangetic plain and peninsular India (Fig. S5c).

Drivers of anomalous moisture transport during ARs. We examined the drivers of increased IVT during ARs in India (Fig. 2). We estimated the dynamic contribution from wind and specific humidity to IVT anomalies during ARs (see methods for details). We find that moisture-carrying wind plays the most prominent role in determining the IVT anomaly during ARs, with about 90% contribution to IVT (Fig. 2a). The remaining 10% is contributed by specific humidity assuming that the nonlinear contribution is negligible (Fig. 2b–d). Both wind speed and specific humidity have significantly (p = 0.001 and 0.009) increased in the summer monsoon season during the 1951–2020 period (Fig. 2e, f). Our results show that the strengthening of moisture-carrying winds and increased specific humidity (Fig. 2e, f) both
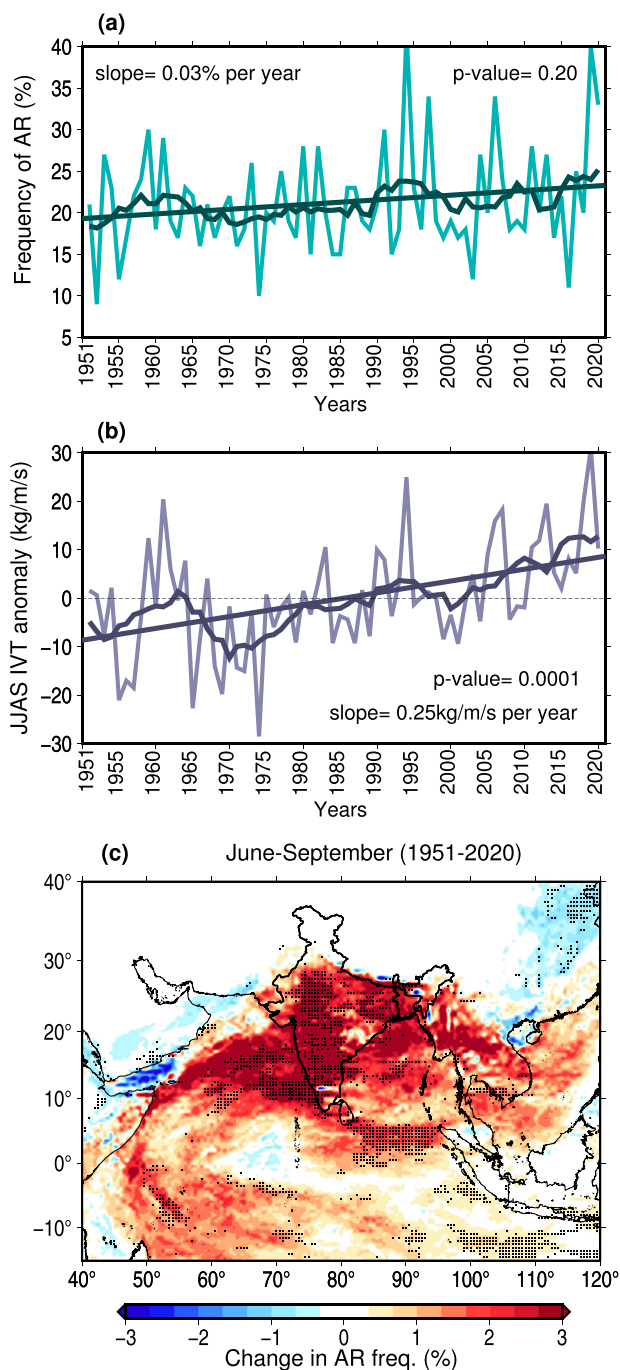
Fig. 1 Changes in atmospheric rivers in India in the summer monsoon season (JJAS, June-September) during 1951–2020. a Trend in the frequency of occurrence of ARs (%) during 1951–2020; **b** Trend in the summer monsoon season IVT anomaly (kg m^{-1} s^{-1}). Solid lines in (**a, b**) indicate the linear trend and 10-year moving mean, respectively; **c** Long-term (1951–2020) change in the frequency of ARs in India. Trend and change (trend slope multiplied by duration) were estimated using the non-parametric Mann-Kendall trend test and Sen slope estimator. Statistical significance was estimated at 5% level, therefore, *p* < 0.05 indicate significant trend/change. Stippling in (**c**) shows the regions with statistically significant change in the frequency of ARs.

contributed to increasing mean summer monsoon IVT in India (Fig. 1b). Area-averaged (40-120E, 10S-25N) IVT anomalies in the summer monsoon season are strongly associated with the strength of the moisture-laden wind (*r* = 0.74). The summer monsoon season is accompanied by low-level (~850 hPa or

2000 km) clouds[35], which are influenced by strong wind and high IVT leading to ARs in India. ARs in the south Asian region are distinguished by high IVT (greater than 500 kg m^{-1} s^{-1}) and river-like structures, which are absent during the regular monsoon episodes[20].

We also examined the thermodynamic drivers contributing to changes in wind and specific humidity anomalies during ARs (Fig. S6). We created composites of mean sea level pressure (MSLP, hPa), vapor pressure deficit (VPD, kPa), and ocean evaporation (ET, mm) anomalies during the ARs in the summer monsoon season for two (1951–1985 and 1986–2020) periods (Fig. S6, S7). Ocean-to-land horizontal pressure gradients prevail during the summer monsoon season, which drives moisture-laden monsoon winds towards the Indian region. MSLP and VPD have significantly increased over the equatorial Indian Ocean in the recent period (1986-2020) compared to 1951-1985 (Fig. S6, S7). The increased VPD anomaly over the Indian Ocean has been attributed to enhanced net radiation[36,37]. Evaporation from the ocean, the predominant monsoon moisture source, has increased due to increased VPD and ocean heat content during the recent period (Fig. S6 and S7). Increased evaporation can also be partly linked with the SST warming over the Indian ocean[38]. Enhanced evaporation from the ocean caused a rise in specific humidity, which led to increased IVT over the Indian region.

The linkage between ARs and flooding in India. To establish the linkage between ARs and flooding, we examined the observed (1985–2020) floods that caused high mortality in India using the Dartmouth Flood Observatory (DFO) database (Fig. 3). Floods included in the DFO over the above period occurred in most regions in India (Fig. S8), especially the Indo-Gangetic Plain, northeastern and central India, and Western Ghats (Fig. 3a). Many regions in India are affected by floods that mostly occur during the summer monsoon season (Fig. 3b). For instance, during each year of the last decade, at least 0.1 million km^2, or more than 3% of the total geographical area of India, has been affected by floods. While floods cause damage to infrastructure and agricultural production and disrupt almost all aspects of human lives, their most devastating impact is human mortality (Fig. 3c, d). In particular, each of the ten floods over the period 1985-2015 caused more than 1000 deaths in India (Fig. 3c, d). Moreover, millions of people have been displaced by major floods in India, mainly in the northeast (Fig. 3e, f). For instance, more than 35 million people were displaced by floods in both 2000 and 2004 (Fig. 3f). Short-duration extreme rainfall and multiday continuous rainfall over wet land surfaces (high antecedent soil moisture) are the major drivers of floods in India[39,40]. Moreover, atmospheric conditions and the availability of moisture sources also favors floods[39]. While floods remain among the deadliest natural disasters in India and are caused mainly by extreme precipitation, it remains unclear the extent to which major floods in India are associated with ARs.

In an attempt to examine the role of ARs in floods during the summer monsoon season in India, we estimated the contribution of ARs to extreme precipitation during the monsoon season. We find that ARs contribute about 13% of India's summer monsoon precipitation (Fig. S9a, b). Their contribution is slightly higher (more than 16%) over central India and western Ghats compared to other parts of India (Fig. S9b). The total precipitation contribution from ARs during the summer monsoon season has significantly (*p* < 0.05) increased during 1951–2020 (Fig. S9c).

India receives almost half of its monsoon precipitation from extreme rainfall events (Fig. S9d), where extreme precipitation is defined as exceeding the 95th percentile of the daily rainfall
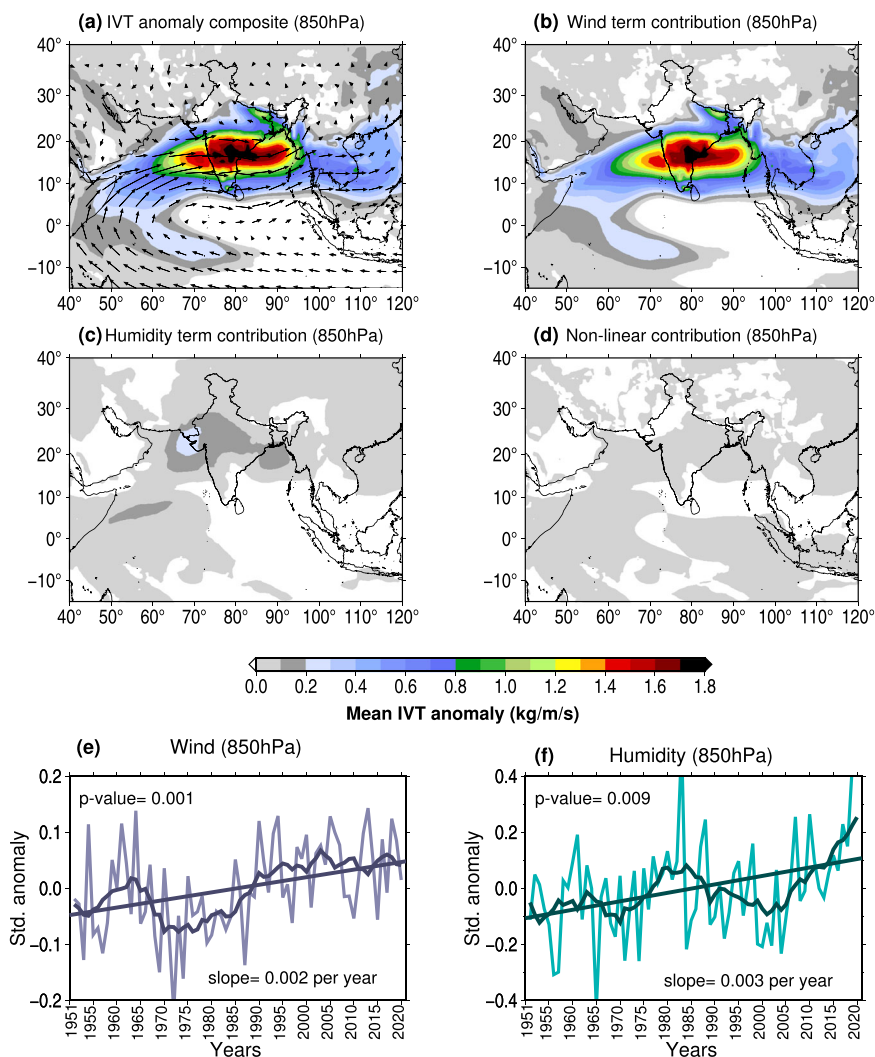
Fig. 2 Major drivers of changes in IVT during 1951–2020. a IVT anomaly composite for atmospheric rivers during the summer monsoon in India at 850hPa level (valid between the 1000–675 hPa range[68]), **b** contribution to IVT from wind at 850hpa, **c** contribution in IVT due to specific humidity, and **d** contribution due to nonlinearity between wind and specific humidity based on the mass decomposition method[67], and (**e**, **f**) trends in standardized anomaly of wind and specific humidity during the summer monsoon season for 1951–2020 period. Lines in (**e**, **f**) represent the linear trend and 10-year moving average. Trend and change (trend slope multiplied by duration) were estimated using the non-parametric Mann-Kendall trend test and Sen slope estimator. Statistical significance was estimated at 5% level, therefore, **p** < 0.05 shows significant trend/change.

distribution. We estimated the fraction of upper 95th percentile daily precipitation associated with ARs during the summer monsoon season. Using this definition, about 18-24% of the total extreme precipitation over the Indian land mass was related to ARs during the 1951–2020 period (Fig. S9e), with a more prominent (~28%) contribution in the Western Ghats and Central India, which can be partly attributed to orography. Orography plays a crucial role in extreme precipitation over the Western Ghats and foothills of the Himalayas[41,42] (also see Fig. S9). High-altitude topographical features promote the uplift of moisture-laden winds that helps ARs to drop moisture and cause extreme precipitation[43–45].

In addition to the statistically significant increase in AR contribution to summer monsoon precipitation, the all-India-averaged extreme precipitation (exceeding 95th percentile) contribution from ARs in the summer monsoon season has also increased (p < 0.05) (Fig. S9f). We note that the extreme precipitation contribution from ARs in the summer monsoon season does not include the contribution from deep depressions and cyclone-like features. Tropical cyclones and deep depressions

(the terms area synonymous) are synoptic-scale features which can also interact with ARs[20]. Cyclonic features mostly evolve in South Asia's pre and post-monsoon seasons[46,47]. Therefore, the extreme precipitation contribution from cyclonic features in the summer monsoon season is negligible[47], and was not considered in our analysis. We used a criterion of circularity greater than 0.5 to exclude deep depression features from our analysis (see methods for details). We also estimated the area affected by extreme precipitation for the days when ARs passed over the Indian landmass. This number (20%, 0.66 million km²) is about double the area affected by extreme precipitation in the absence of ARs (Fig. S10). The larger area of extreme precipitation associated with ARs results from the larger area of AR-related extreme precipitation events[3,48]. Our results show that the variability in the area of AR-related extreme precipitation is strongly associated with the changes in winds and humidity during the summer monsoon season (Fig. 2e, f). Overall, extreme precipitation from ARs and the associated affected area has increased significantly during the summer monsoon season in India over the period 1951–2020 (p < 0.05).
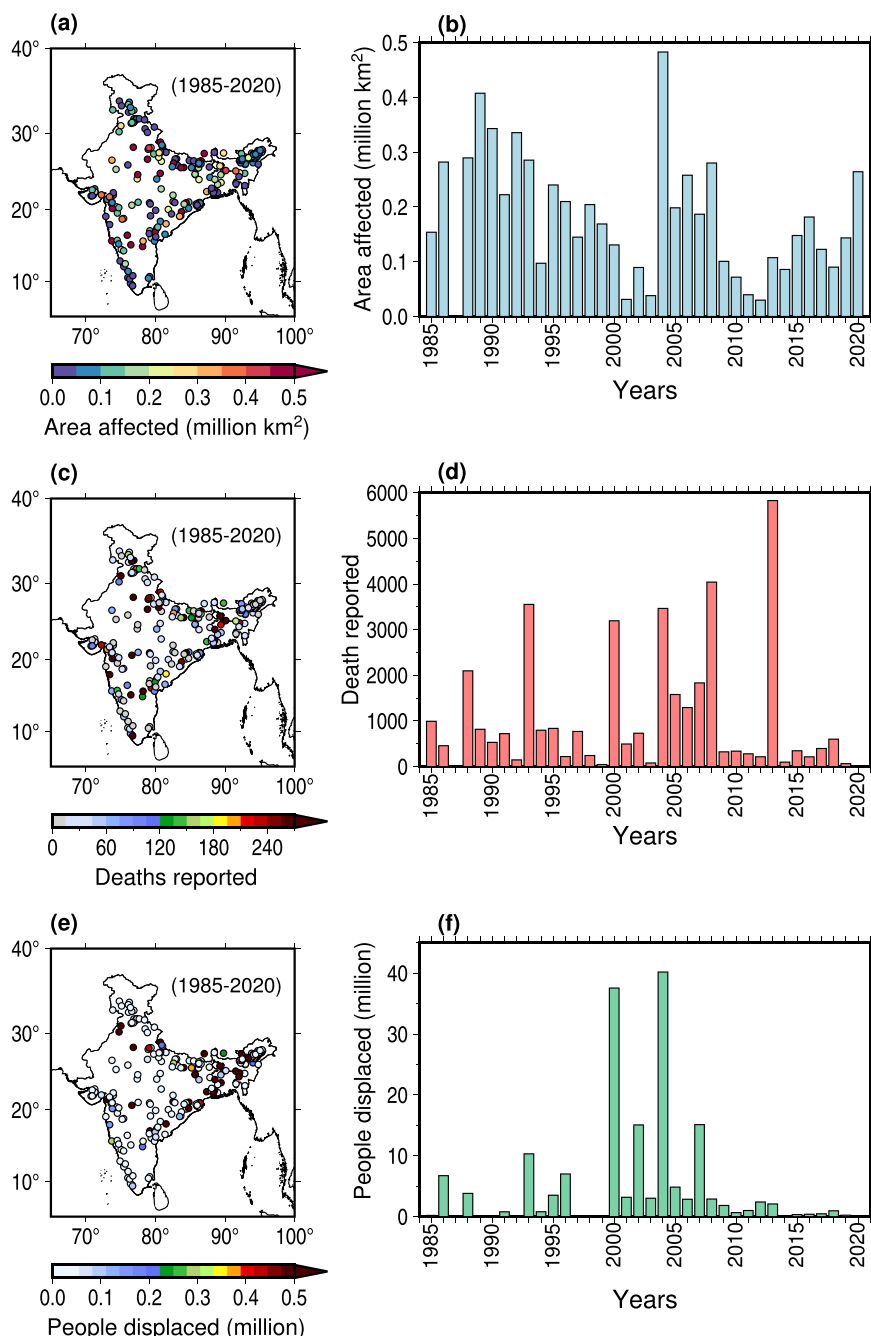
Fig. 3 Major floods during the summer monsoon season (June-September) in India during 1985–2020. a Flood locations with color scale representing the total geographical area affected (in million km²). **b** Average area affected by floods during 1985–2020. **c** Deaths reported due to the major floods along with their locations. **d** Total deaths reported each year during 1985–2020. **e** People displaced due to floods and their locations. **f** Total population displaced each year due to floods. The major flood data base was obtained from the Dartmouth Flood Observatory, University of Colorado, USA (available at https://floodobservatory.colorado.edu/Archives/index.html).

Finally, we examined the role of ARs in India's ten greatest floods during 1985–2020 (Fig. S11, Table S1). We identified the ten largest floods based on flood severity and the number of deaths (see methods for details) reported by the Dartmouth Flood Observatory (DFO) for the period 1985–2020. The fraction of ARs that cause floods (flood-associated ARs) was based on floods that were reported (in the DFO flood database) and overlapped with the AR-affected area during the flood event (Fig. 4a, b; Supplemental Data 1). A total of 292 ARs occurred in the summer monsoon season (1985–2020), or an average of 49 ARs per six years, of which 65% (~32 ARs) were associated with floods

(Fig. 4a). The percentage of flood-associated ARs in last two decade is nearly 72% (Fig. 4a). Among the most severe ARs (top 1/3rd) in post 1985 period, 63 AR events occurred in the last two decades (after 2003) [Fig. S12b], of which 82% (~52 ARs) were associated with floods (Fig. 4b). Moreover, severity of flood-associated ARs was higher in the last two decades (2003–2020) compared to flood-associated ARs in the 1985-2002 period (Fig. 4c). We do note that while the above statistics are suggestive of trends, the changes in the frequency and severity of the flood associated ARs are not statistically significant for our 1985–2020 analysis period.
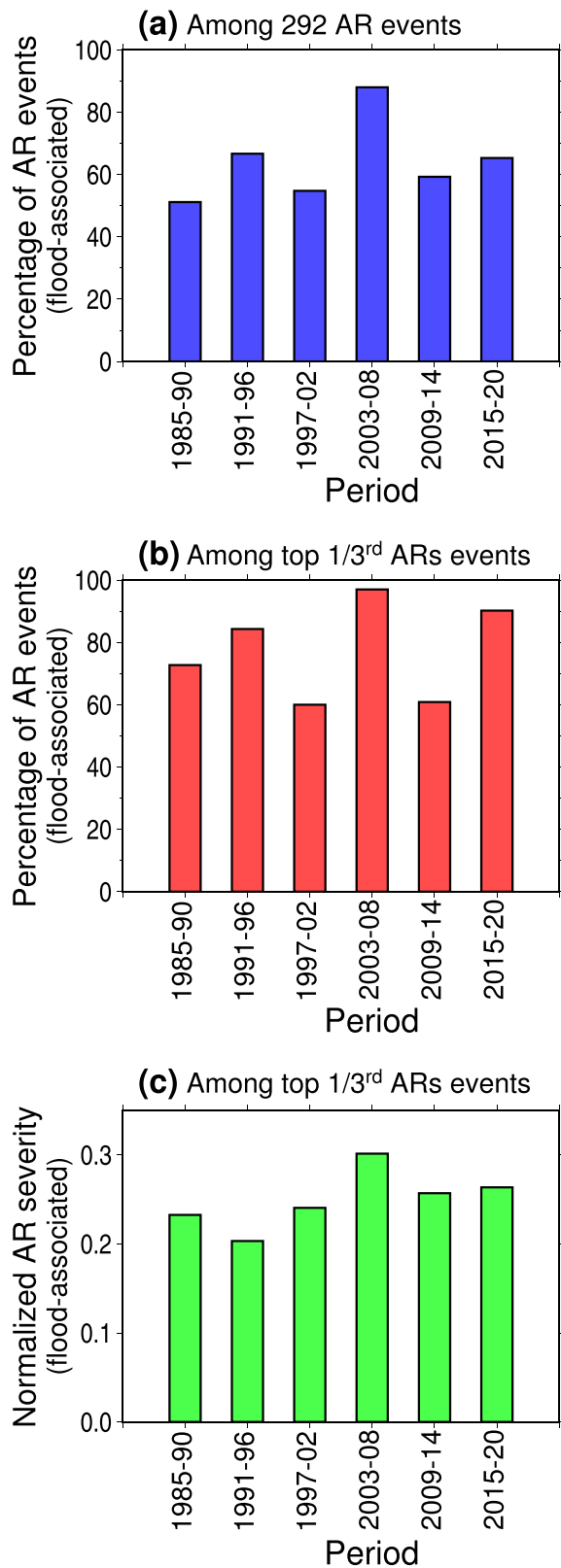
Fig. 4 Flood associated atmospheric rivers in India during 1985–2020. a Percentage of flood-associated AR events during 1985–2020 period (flood database was only available for the post 1985 period). A total of 292 AR events were identified between 1985 and 2020. **b** Percentage of flood-associated ARs among the top 1/3rd events (~100) in the 1985–2020 period, sorted by decreasing order of severity score (see Eq. 4 for details). **c** Normalized mean severity score of flood-associated AR events for the top 1/3rd events during the1985–2020 period. ARs were identified using ERA5 reanalysis. Database of major floods in India was compiled using the number of deaths reported during each flood in the Dartmouth Flood Observatory, University of Colorado, USA (available at https://floodobservatory.colorado.edu/Archives/index.html).

associated rainfall during the two highest rainfall days (16-17th June 2013) dropped more than 350 mm (375% departure from the long-term mean) of rainfall over the Uttarakhand region (Fig. S11a-c) with a 3-day accumulated rainfall of more than 400 mm over the region[50]. This event triggered landslides and flash floods[49,51,52]. An unabated supply of moisture from the Indo-Gangetic branch of the AR was one of the main drivers of the extreme precipitation over north India in this event.

ARs also caused floods in 2007 (July-August) and 1988 (September), with extreme loss of life over the eastern and north-western parts of India (Fig. S11e, h). The extent of flood impacts in the 2007 event was spread across the South Asian countries, including India, taking the lives of more than 2000 people[53]. Similarly, the September 1988 event, caused by an AR, led to especially disastrous floods in the Punjab state[54]. The other two major flood events that led to extreme loss of life affected the western peninsular regions of India. The Kerala flood in August 2018 took the lives of over 400 people and displaced a million more[55,56]. The anomalous moisture supplied by the August 2018 event caused massive flooding. The southern part of Gujarat experienced the worst flood of record due to the August 2006 AR, which inundated more than 80% of Surat City[57]. The Indo-Gangetic plain and Assam witnessed more than 500 deaths and agricultural damage caused by extreme rainfall due to an AR in July 1993[58]. The Nepal region experienced record-breaking precipitation in July 1993 caused by an AR[59]. Similarly, AR in 2004 contributed to hazardous floods in Eastern India and Bangladesh that affected the lives and property of about 70 million people[60]. Other major flood events in the summer monsoon season associated with landfalling ARs occurred in 2000, 2008, and 1985. Overall, 70% of India's major flood events in the summer monsoon season were directly associated with ARs during the 1985–2020 period.

Conclusions

We examined landfalling ARs during the summer monsoon, which has implications for water resources and deleterious flood hazards in India since they can deliver enormous amounts of precipitation within a few hours or days[9,13,31]. A warming climate is increasing the moisture-holding capacity of ARs[10,28,61], which leads to concerns about more devastating floods in the future. The ARs predominantly occur in the summer monsoon season in India, which passes through the Indian sub-continent from west to east. A total of 574 ARs occurred in the summer monsoon season during 1951–2020, with the frequency of ARs increasing over time. Moreover, in the last two decades, nearly 80% of the most severe ARs (top 1/3rd AR events, Supplemental Data 1) caused floods in India. Warmer SSTs over the south-central Indian Ocean play a crucial role in the development of ARs. Evaporation from the Indian Ocean has significantly increased in recent decades due to an increase in VPD. The frequency of ARs and floods caused by them has increased recently as the climate has warmed. Floods have

Out of the ten floods during 1985–2020 that caused the highest mortality, seven (in 2013, 2007, 1988, 2018, 2006, 1993, and 2004) were associated with ARs (Fig. S11, Table S1). These floods caused the loss of more than 9000 human lives and billions of US dollars in damage (Global Active Archive of Large Flood Events, DFO). The most devastating flood during 12-27th June 2013 in Uttarakhand alone took around 6000 human lives[49]. AR-

devastating impacts on the economy and society[62–64], and understanding the role of ARs in the observed and projected future climate is crucial in mitigating the flood risks. In addition, ARs should be an integral part of the existing flood early warning systems in India, which can help in adaptation and mitigation.

Data and methods

Hydrometeorological data. We used vertically integrated water vapor transport (IVT) to identify atmospheric rivers (ARs) over India [40°E to 120°E and −15°S to 40°N] for the 1951–2020 period. We computed IVT (kg m^{-1} s^{-1}) using the vertical integral of eastward and northward water vapor flux collected from the 5th generation European Centre for Medium-Range Weather Forecasts (ECMWF) Reanalysis [ERA5[25]] as:

$$IVT = \sqrt{q_u^2 + q_v^2} \quad (1)$$

Where q_u and q_v are the vertical integrals of eastward and northward water vapor flux derived from ERA5 reanalysis, respectively. ERA5 integrates q_u and q_v over the pressure levels between the surface (~1000 hPa) and the top of the 18 km thick atmosphere (~10 hPa). We used the ERA5 reanalysis because it has been shown to perform better than other reanalysis products for hydrological and meteorological applications in the Indian region[65,66]. We used specific humidity (q), u, and v components of wind at 850 hPa from the ERA5 reanalysis to examine the dynamic mechanism of atmospheric rivers in the Indian region. We used 2 m surface air temperature (T) and dew point temperature (DPT) from ERA5 reanalysis to estimate vapor pressure deficit (VPD) over the land and the Indian Ocean. We also used ocean evaporation (ET) and mean sea level pressure (MSLP) from ERA5 to examine the thermodynamic mechanisms of ARs. We applied a dynamic mass decomposition method[67] to estimate the individual contributions of wind and humidity in generating the moisture flux magnitude (IVT). The decomposition method (Eq. 2) describes the change (anomaly) in IVT as a function of the fractional change in the wind and specific humidity. The decomposition of the moisture flux anomaly was obtained as:

$$(qw)' = \bar{q}w' + q'\bar{w} + q'w' \quad (2)$$

where w and q are the wind velocity (m s^{-1}) and specific humidity (kg kg^{-1}) at 850 hPa level, respectively. The overbar and prime denote the long-term climatological mean and anomaly, respectively. Equation 2 represents a section of IVT at 850 hPa, which is the average height (~2000 m) of monsoonal moisture flow[35]. Due to the limitation of vertically integrated components of wind and specific humidity, we used wind (w) and humidity (q) at 850 hPa to examine the dynamics of ARs. The wind and humidity variables reach their maximum at or near 850 hPa between the layers from 1000 hPa to 675 hPa as in[68]. Thus, $(qw)'$ represents the IVT anomaly estimated between 1000 and 675 hPa pressure levels. Similarly, $\bar{q}w'$ and $q'\bar{w}$ represent the linear contribution from w and q anomalies, respectively, whereas $q'w'$ represents the nonlinear (combination of both q and w) contributions to the anomalous moisture flux. The wind and specific humidity from ERA5 are considered reliable over spatial and temporal scales[69]. For instance, ERA5 reproduces wind speed and humidity reliably compared with ground observations and radiosonde measurements[70–72].

Similarly, we used precipitation (P) from ERA5 to estimate extreme rainfall and flood severity associated with ARs over India. We also used observed precipitation from the India Meteorological Department (IMD) to evaluate the robustness of the ERA5 reanalysis in capturing extreme rainfall during flood events (Fig. S11). We used the zonal (east-west) and meridional (north-south) wind components from ERA5 reanalysis at 850 hPa

to estimate the direction of moisture flow in the AR, which is the similar as directions given by the resultant of q_u and q_v.

Identification of ARs in India. We used a daily threshold IVT magnitude to identify landfalling ARs[18,73,74]. The continuous transport of water vapor by monsoonal flow in south Asia usually persists for more than a day and can have associated IVT of up to 350 kg m^{-1} s^{-1}. A fixed IVT threshold (250 kg m^{-1} s^{-1}) generates a preliminary cluster of large area due to high monsoonal flow (Fig. S13), which may increase the frequency of occurrence of AR at each grid (Fig. S14). The large area of the identified cluster may not fulfill all the conditions required to be categorized as an AR[75]. Moreover, despite high monsoonal flow, IVT has substantial spatial variations across India, especially over the high-altitude and arid regions, where IVT is limited to about 150 kg m^{-1} s^{-1}[76]. Therefore, we used a threshold of the 85th percentile of the daily IVT for each grid instead of taking a fixed threshold of IVT to account for the large spatial variability in IVT[27]. A recent study[20] emphasized that ARs over the Indian region have a big seasonal difference in IVT magnitude. Therefore, these deserve investigation using a modified AR identification algorithm specific to the monsoonal region. We developed an algorithm to detect ARs in the south Asian region using the methodology presented in the recent studies[20,27,30,34].

Initially, we identified the grid cells with IVT each day that exceeded the 85th percentile of IVT. To estimate the climatological mean IVT of a given day, we used a moving window of 15 days (7 days before, current day, and seven days after) for the 1951–2020 period to avoid short-term fluctuations. Additionally, we required the 85th percentile IVT to be greater than 150 kg m^{-1} s^{-1} to confirm the higher strength of moisture transport in ARs[27]. The average monthly mean IVT magnitude for each month was higher than 150 kg m^{-1} s^{-1} (Fig. S1b), which was the criteria for selecting the threshold. We made contiguous clusters from the selected grids identified using the threshold. The clusters were identified using the Image Segmentation Toolbox in MATLAB from the daily IVT (>85th percentile and >150 kg m^{-1} s^{-1}) layer, which was converted to a binary image before processing. Small clusters were removed if a cluster had less than 500 grids. The remaining clusters of grid cells in the study region were flagged as preliminary ARs. Clusters of IVT that either did not pass over India's land part or had a lesser area (~50,000 km^2) were not considered as preliminary ARs.

We implemented two additional criteria to distinguish tropical moisture flow (general monsoonal flow) from the ARs in the south Asian region, as suggested in previous studies[20,77]. The cluster of a preliminary AR was neglected if the grids in the extra tropical region (beyond the 20°N latitude) covered less than 5% of the total area of preliminary AR. We implemented this step to remove east-west oriented moisture swells south of 20°N and to preserve the AR characteristics of extra-tropical moisture transport[20]. In the next step, we ensured that more than 50% of the AR grids in the tropical region (20°N-20°S) should have IVT direction more than 15°, as this criterion removes the clusters that are in the tropics with minimum poleward component[20]. Furthermore, to ensure that the severity of landfalling ARs remains high to produce extreme precipitation leading to flood, we considered only those clusters that had mean IVT greater than 500 kg m^{-1} s^{-1} over the Indian landmass.

The geometric conditions we used for AR identification were length greater than 2000 km and length to width ratio (LWratio) greater than two. The AR length was calculated by joining the grids of maximum meridional IVT within a qualified cluster[27,30]. AR width was defined as the ratio of area to length, which was also used to calculate the LW ratio for isolated contiguous clusters. Deep depressions (moderate low-pressure systems) are

sometimes expected during the summer monsoon season over the Indian region and should not be confused with atmospheric rivers[31]. ARs are more narrow and linear features, whereas cyclones have circular features. Therefore, the clusters of preliminary atmospheric rivers with circularity greater than 0.5 (circularity = 1 represents a full circle) and eccentricity less than 0.5 (eccentricity = 1 represents a linear shape) were excluded from our analysis. Finally, the clusters preliminary ARs that satisfied all the set criteria were considered the final ARs. Persistent ARs for two days or more were considered as a single AR event, where the total number of continuous days of an event was the duration of the AR.

AR frequency and ranking criteria. We estimated the frequency of ARs for each grid cell rather than just counting the AR days. For a particular grid cell, we estimated the number of days for which an AR was detected and passed over that grid cell. Therefore, the AR frequency (% of time-step) is the number of days for which an AR passed over the grid cell divided by the total number of days during the 1951–2020 period (Eq. 3)[77,78]. We ranked the atmospheric rivers based on their severity scores (Eq. 4). The severity score is defined as the product of the areal extent of an AR over land and its average IVT intensity over land (taking the temporal mean if an AR has a duration of more than a day). We normalized both the AR area and IVT intensity over land on a scale of zero to one, keeping input parameters within a consistent range and dimensionless before estimating the AR severity score. The severity score measures the combined impact of AR intensity and areal extent over the Indian landmass.

$$AR\ frequency\ at\ a\ grid\ cell\,(\%) = \frac{Number\ of\ days\ with\ AR\ passes}{total\ number\ of\ days} \times 100 \quad (3)$$

$$AR\ severity\ score\ = normalize\,(ARs\ area\ over\ land) \\ \times normalize\,(average\ IVT\ over\ land) \quad (4)$$

Extreme precipitation and major floods from ARs. Extreme daily precipitation is considered to have occurred when the rainfall for a particular day exceeds the 95th percentile (the threshold for extreme rainfall based on days with rainfall exceeding 1 mm) for the entire 1951–2020 period for a given grid cell. Since most AR occurs during the monsoon season (JJAS; June to September), we considered only those days that experienced an AR over a grid cell during the summer monsoon season. We estimated the total monsoon season precipitation contribution from ARs, extreme precipitation contribution from ARs, and average area (number of grids × 50 km ×50 km) that experienced extreme precipitation each year from 1951–2020. We used the nonparametric Mann-Kendall trend[79] and Sen slope estimator[80] to identify trends (at the 5% significance level) in the summer monsoon season.

We identified major flood events in India during 1985–2020 from the Dartmouth Flood Observatory (DFO), University of Colorado, USA (available at https://floodobservatory.colorado.edu/Archives/index.html). DFO provides country-wise flood-related details (location, area, began and end date, validation source, death reported, people displaced, primary cause, and flood severity) of major flood events (any flood with substantial damage to properties, infrastructures or agriculture, and fatalities) from 1985 onwards. DFO assigns three flood severity classes. Class 1 are large flood events with a 10–20 years return period. Severity class 1.5 are very large events with 20–100 years of return period, and/or a local recurrence interval of at 1-2 decades and affecting a large geographic region (>5000 sq. km). Similarly, class 2 severity indicates extreme flood events with an estimated recurrence interval greater than 100 years. The flood database provides a long-term archive of major flood details for quick analysis; however, there can be uncertainties in the beginning and end dates (DFO). For instance, when only a month is reported in the validation sources; DFO flood beginning date will be the middle of that month and the same for the end date.

Since most annual precipitation occurs during the summer monsoon season in India, we considered only flood events that occurred during the monsoon season. We selected monsoon season floods with DFO severity greater than or equal to 1.5 (DFO severity = 1.5 and 2 indicate very large and extreme flood events, respectively; see Table S1). Finally, we ranked all the monsoon season floods based on the number of deaths (maximum casualty indicated by rank 1) and selected the ten most severe flood events for further analysis. The ten most severe flood events in the summer monsoon season in India that caused the highest causalities and had a severity of more than 1.5 were selected (Table S1). We also assembled a catalog of ARs during 1951–2020 with characteristics such as length, area, duration, mean and maximum IVT magnitude, land area affected, and flood association, if any (Supplemental Data 1). The catalog provides information about the occurrence and historical characteristics of ARs in India. In addition, the ARs and corresponding floods caused by them can also be identified. Similarly, a separate list for ARs in the non-monsoon season is also provided (Table S2). However, our analysis mainly focused on the ARs in the summer monsoon season.

References
1. Banerji, U. S., Arulbalaji, P. & Padmalal, D. Holocene climate variability and Indian Summer Monsoon: an overview. *SAGE J.* https://doi.org/10.1177/0959683619895577 (2020).
2. Mishra, V., Smoliak, B. V., Lettenmaier, D. P. & Wallace, J. M. A prominent pattern of year-to-year variability in Indian Summer Monsoon Rainfall. *Proc. Natl. Acad. Sci. USA* **109**, 7213–7217 (2012).
3. Mukherjee, S., Aadhar, S., Stone, D. & Mishra, V. Increase in extreme precipitation events under anthropogenic warming in India. *Weather Clim. Extrem.* **20**, 45–53 (2018).
4. Nikumbh, A. C., Chakraborty, A. & Bhat, G. S. Recent spatial aggregation tendency of rainfall extremes over India. *Sci. Rep.* **9**, 1–7 (2019).
5. Goswami, B. N. & Xavier, P. K. ENSO control on the south Asian monsoon through the length of the rainy season. *Geophys. Res. Lett.* **32**, 1–4 (2005).
6. Ali, H. & Mishra, V. Increase in subdaily precipitation extremes in India under 1.5 and 2.0 °C warming worlds. *Geophys. Res. Lett.* **45**, 6972–6982 (2018).
7. Roxy, M. K. et al. A threefold rise in widespread extreme rain events over central India. *Nat. Commun.* **8**, 1–11 (2017).
8. Dettinger, M. D., Ralph, F. M., Das, T., Neiman, P. J. & Cayan, D. R. Atmospheric rivers, floods and the water resources of California. *Water* **3**, 445–478 (2011).
9. Cao, Q. et al. Floods due to atmospheric rivers along the U.S. West coast: the role of antecedent soil moisture in a warming climate. *J. Hydrometeorol.* **21**, 1827–1845 (2020).

10. Algarra, I. et al. Significant increase of global anomalous moisture uptake feeding landfalling atmospheric rivers. *Nat. Commun.* **11**, 1–7 (2020).

11. Corringham, T. W., Martin Ralph, F., Gershunov, A., Cayan, D. R. & Talbot, C. A. Atmospheric rivers drive flood damages in the western United States. *Sci. Adv.* **5**, eaax4631 (2019).

12. Lavers, D. A. & Villarini, G. Atmospheric rivers and flooding over the central United States. *J. Clim.* **26**, 7829–7836 (2013).

13. Ralph, F. M. et al. Flooding on California's Russian river: role of atmospheric rivers. *Geophys. Res. Lett.* https://doi.org/10.1029/2006GL026689 (2006).

14. Lavers, D. A. & Villarini, G. The contribution of atmospheric rivers to precipitation in Europe and the United States. *J. Hydrol.* **522**, 382–390 (2015).

15. Lavers, D. A. & Villarini, G. The nexus between atmospheric rivers and extreme precipitation across Europe. *Geophys. Res. Lett.* **40**, 3259–3264 (2013).

16. Guan, B. & Waliser, D. E. Tracking atmospheric rivers globally: spatial distributions and temporal evolution of life cycle characteristics. *J. Geophys. Res. Atmos.* **124**, 12523–12552 (2019).

17. Martin Ralph, F. et al. A scale to characterize the strength and impacts of atmospheric rivers. *Bull. Am. Meteorol. Soc.* **100**, 269–289 (2019).

18. Espinoza, V., Waliser, D. E., Guan, B., Lavers, D. A. & Ralph, F. M. Global analysis of climate change projection effects on atmospheric rivers. *Geophys. Res. Lett.* **45**, 4299–4308 (2018).

19. Payne, A. E. et al. Responses and impacts of atmospheric rivers to climate change. *Nat. Rev. Earth Environ.* **1**, 143–157 (2020).

20. Pan, M. & Lu, M. East asia atmospheric river catalog: annual cycle, transition mechanism, and precipitation. *Geophys. Res. Lett.* **47**, e2020GL089477 (2020).

21. Katzenberger, A., Schewe, J., Pongratz, J. & Levermann, A. Robust increase of Indian monsoon rainfall and its variability under future warming in CMIP6 models. *Earth Syst. Dyn.* **12**, 367–386 (2021).

22. Dhana Lakshmi, D. & Satyanarayana, A. N. V. Influence of atmospheric rivers in the occurrence of devastating flood associated with extreme precipitation events over Chennai using different reanalysis data sets. *Atmos. Res.* **215**, 12–36 (2019).

23. Lyngwa, R. V. & Nayak, M. A. Atmospheric river linked to extreme rainfall events over Kerala in August 2018. *Atmos. Res.* **253**, 105488 (2021).

24. Ali, H., Modi, P. & Mishra, V. Increased flood risk in Indian sub-continent under the warming climate. *Weather Clim. Extreme.* **25**, 100212 (2019).

25. Hersbach, H. et al. The ERA5 global reanalysis. *Q. J. R. Meteorol. Soc.* **146**, 1999–2049 (2020).

26. Pai, D. S., Rajeevan, M., Sreejith, O. P., Mukhopadhyay, B. & Satbha, N. S. Development of a new high spatial resolution (0.25° × 0.25°) long period (1901–2010) daily gridded rainfall data set over India and its comparison with existing data sets over the region. *MAUSAM* **65**, 1–18 (2014).

27. Guan, B. & Waliser, D. E. Detection of atmospheric rivers: evaluation and application of an algorithm for global studies. *J. Geophys. Res. Atmos.* **120**, 12514–12535 (2015).

28. Rhoades, A. M., Risser, M. D., Stone, D. A., Wehner, M. F. & Jones, A. D. Implications of warming on western United States landfalling atmospheric rivers and their flood damages. *Weather Clim. Extreme.* **32**, 100326 (2021).

29. Dhana Laskhmi, D. & Satyanarayana, A. N. V. Climatology of landfalling atmospheric Rivers and associated heavy precipitation over the Indian coastal regions. *Int. J. Climatol.* **40**, 5616–5633 (2020).

30. Liang, J. & Yong, Y. Climatology of atmospheric rivers in the Asian monsoon region. *Int. J. Climatol.* **41**, E801–E818 (2021).

31. Lakshmi, D. D., Satyanarayana, A. N. V. & Chakraborty, A. Assessment of heavy precipitation events associated with floods due to strong moisture transport during summer monsoon over India. *J. Atmos. Solar-Terrestrial Phys.* **189**, 123–140 (2019).

32. Leung, L. R. & Qian, Y. Atmospheric rivers induced heavy precipitation and flooding in the western U.S. simulated by the WRF regional climate model. *Geophys. Res. Lett.* **36**, n/a–n/a (2009).

33. Francis, D., Mattingly, K. S., Temimi, M., Massom, R. & Heil, P. On the crucial role of atmospheric rivers in the two major Weddell Polynya events in 1973 and 2017 in Antarctica. *Sci. Adv.* **6**, eabc2695 (2020).

34. Pan, M. & Lu, M. A novel atmospheric river identification algorithm. *Water Resour. Res.* **55**, 6069–6087 (2019).

35. Varikoden, H. et al. Properties of cloud base height during southwest monsoon period over a tropical station, Thiruvananthapuram. *Curr. Sci.* **96**, 562–568 (2009).

36. Wang, G. et al. The causality from solar irradiation to ocean heat content detected via multi-scale Liang-Kleeman information flow. *Nature.* https://doi.org/10.1038/s41598-020-74331-2 (2020).

37. Loeb, N. G. et al. Satellite and ocean data reveal marked increase in Earth's heating rate. *Geophys. Res. Lett.* https://doi.org/10.1029/2021GL093047 (2021).

38. Roxy, M. K. et al. Drying of Indian subcontinent by rapid Indian Ocean warming and a weakening land-sea thermal gradient. *Nat. Commun.* **6**, 1–10 (2015).

39. Nanditha, J. S., Rajagopalan, B. & Mishra, V. Combined signatures of atmospheric drivers, soil moisture, and moisture source on floods in Narmada River basin, India. *Clim. Dyn.* **59**, 2831–2851 (2022).

40. Nanditha, J. S. & Mishra, V. Multiday precipitation is a prominent driver of floods in Indian River basins. *Water Resour. Res.* https://doi.org/10.1029/2022WR032723 (2022).

41. Goswami, B. B., Mukhopadhyay, P., Mahanta, R. & Goswami, B. N. Multiscale interaction with topography and extreme rainfall events in the northeast Indian region. *J. Geophys. Res.* https://doi.org/10.1029/2009JD012275 (2010).

42. Krishnamurti, T. N. et al. March of buoyancy elements during extreme rainfall over India. *Clim. Dyn.* **48**, 1931–1951 (2017).

43. Neiman, P. J. et al. The landfall and inland penetration of a flood-producing atmospheric river in Arizona. Part I: observed synoptic-scale, orographic, and hydrometeorological characteristics. *J. Hydrometeorol.* **14**, 460–484 (2013).

44. Neiman, P. J., Ralph, F. M., Moore, B. J. & Zamora, R. J. The regional influence of an intense Sierra barrier jet and landfalling atmospheric river on orographic precipitation in northern California: a case study. *J. Hydrometeorol.* **15**, 1419–1439 (2014).

45. Mo, R. et al. Impacts of hydrometeor drift on orographic precipitation: two case studies of landfalling atmospheric rivers in British Columbia, Canada. *Weather Forecast.* **34**, 1211–1237 (2019).

46. Muni Krishna, K. Intensifying tropical cyclones over the North Indian Ocean during summer monsoon—Global warming. *Glob. Planet. Chang.* **65**, 12–16 (2009).

47. Singh, K., Panda, J., Osuri, K. K. & Vissa, N. K. *Recent Developments in Tropical Cyclone Dynamics, Prediction, and Detection* (InTech, 2016).

48. Pattanaik, D. R. & Rajeevan, M. Variability of extreme rainfall events over India during southwest monsoon season. *Meteorol. Appl.* **17**, 88–104 (2010).

49. Martha, T. R. et al. Landslides triggered by the June 2013 extreme rainfall event in parts of Uttarakhand state, India. *Landslides* **12**, 135–146 (2015).

50. Srivastava, A. K. & Guhathakurta, P. *Climate Diagnostics Bulletin of India.* http://www.indiaenvironmentportal.org.in/content/446964/climate-diagnostics-bulletin-of-india/ (2013).

51. Ray, P. K. et al. *Kedarnath Disaster 2013: Causes and Consequences Using Remote Sensing Inputs. Nat. Hazards* **81**, 227–224 (2016).

52. Houze, R. A., McMurdie, L. A., Rasmussen, K. L., Kumar, A. & Chaplin, M. M. Multiscale aspects of the storm producing the June 2013 flooding in Uttarakhand, India. *Mon. Weather Rev.* **145**, 4447–4466 (2017).

53. Forbes. *South Asia Floods Death Toll Passes 2,000; India Releases Disaster Relief.* http://www.forbes.com/markets/feeds/afx/2007/08/09/afx4003968.html (2022).

54. ReliefWeb. India floods Oct 1988 {UNDRO} information Report 1. https://reliefweb.int/report/india/india-floods-oct-1988-undro-information-report-1 (1988).

55. Hunt, K. M. R. & Menon, A. The 2018 Kerala floods: a climate change perspective. *Clim. Dyn.* **54**, 2433–2446 (2020).

56. Mishra, V. & Shah, H. L. Hydroclimatological perspective of the Kerala flood of 2018. *J. Geol. Soc. India 2018 925* **92**, 645–650 (2018).

57. Mavalankar D. & Srivastava A. K. Lessons from Massive Floods of 2006 in Surat City: A framework for Application of MS/OR Techniques to Improve Dam Management to Prevent Flood. *IIM Ahmedabad.* https://iima.ac.in/sites/default/files/rnpfiles/2008-07-06Mavalankar.pdf (2008).

58. Preet, J. *No Lesson Learnt From 1993 Floods.* https://timesofindia.indiatimes.com/city/chandigarh/no-lesson-learnt-from-1993-floods/articleshow/3456700.cms (2022).

59. Mirza, M. M. Q. Climate change, flooding in South Asia and implications. *Reg. Environ. Chang.* **11**, 95–107 (2011).

60. Ali, A. M. S. September 2004 flood event in southwestern Bangladesh: a study of its nature, causes, and human perception and adjustments to a new hazard. *Nat. Hazards* **40**, 89–111 (2004).

61. Corringham, T. W. et al. Climate change contributions to future atmospheric river flood damages in the western United States. *Sci. Rep.* **12**, 13747 (2022).

62. Merz, B. et al. Causes, impacts and patterns of disastrous river floods. *Nat. Rev. Earth Environ. 2021 29* **2**, 592–609 (2021).

63. Svetlana, D., Radovan, D. & Ján, D. The economic impact of floods and their importance in different regions of the World with emphasis on Europe. *Procedia Econ. Financ.* **34**, 649–655 (2015).

64. Dewan, T. H. Societal impacts and vulnerability to floods in Bangladesh and Nepal. *Weather Clim. Extreme.* **7**, 36–42 (2015).

65. Mahto, S. S. & Mishra, V. Does ERA-5 outperform other reanalysis products for hydrologic applications in India? *J. Geophys. Res. Atmos.* **124**, 9423–9441 (2019).

66. Dullaart, J. C. M., Muis, S., Bloemendaal, N. & Jeroen Aerts, C. J. H. Advancing global storm surge modelling using the new ERA5 climate reanalysis. *Clim. Dyn.* **54**, 1007–1021 (2020).

67. Sekizawa, S. et al. Anomalous moisture transport and oceanic evaporation during a torrential rainfall event over Western Japan in Early July 2018. *SOLA* **15**, 15A–005 (2019).

68. Baek, S. H. & Lora, J. M. Counterbalancing influences of aerosols and greenhouse gases on atmospheric rivers. *Nat. Clim. Chang.* **11**, 958–965 (2021).

69. Olauson, J. ERA5: The new champion of wind power modelling? *Renew. Energy* **126**, 322–331 (2018).

70. Mateus, P., Mendes, V. B., Plecha, S. M., Bonafoni, S. & Luiz, I. D. HGPT2: An ERA5-based global model to estimate relative humidity. *Remote Sens.* **13**, 2179 (2021).

71. Molina, M. O., Gutiérrez, C. & Sánchez, E. Comparison of ERA5 surface wind speed climatologies over Europe with observations from the HadISD dataset. *Int. J. Climatol.* **41**, 4864–4878 (2021).

72. Alghamdi, A. S. Evaluation of four reanalysis datasets against radiosonde over Southwest Asia. *Atmos.* **11**, 402 (2020).

73. Gershunov, A. et al. Precipitation regime change in Western North America: the role of atmospheric rivers. *Sci. Rep.* **9**, 1–11 (2019).

74. Rutz, J. J., James Steenburgh, W. & Martin Ralph, F. Climatological characteristics of atmospheric rivers and their inland penetration over the western united states. *Mon. Weather Rev.* **142**, 905–921 (2014).

75. Reid, K. J., King, A. D., Lane, T. P. & Short, E. The sensitivity of atmospheric river identification to integrated water vapor transport threshold, resolution, and regridding method. *J. Geophys. Res.* https://doi.org/10.1029/2020JD032897 (2020).

76. Mattingly, K. S., Mote, T. L. & Fettweis, X. Atmospheric river impacts on greenland ice sheet surface mass balance. *J. Geophys. Res. Atmos.* **123**, 8538–8560 (2018).

77. Mundhenk, B. D., Barnes, E. A. & Maloney, E. D. All-season climatology and variability of atmospheric river frequencies over the North Pacific. *J. Clim.* **29**, 4885–4903 (2016).

78. Li, C., Mei, W. & Kamae, Y. Variability and predictability of cold-season North Atlantic atmospheric river occurrence frequency in a set of high-resolution atmospheric simulations. *Clim. Dyn.* **58**, 2485–2500 (2022).

79. Mann, H. B. Nonparametric tests against trend. *Econometrica* **13**, 245 (1945).

80. Sen, P. K. Estimates of the regression coefficient based on Kendall's Tau. *J. Am. Stat. Assoc.* **63**, 1379–1389 (1968).

Acknowledgements

Author contributions

V.M and S.S.M. designed and conceptualized the study. S.S.M. wrote the first draft, V.M., D.P.L., and M.A.N. contributed to the discussion.

Competing interests

The authors declare no competing interests.

Additional information

Supplementary information The online version contains supplementary material available at https://doi.org/10.1038/s43247-023-00775-9.

Correspondence and requests for materials should be addressed to Vimal Mishra.

Peer review information *Communications Earth & Environment* thanks Tom Corringham, Ruping Mo and the other, anonymous, reviewer(s) for their contribution to the peer review of this work. Primary Handling Editors: Akintomide Akinsanola and Heike Langenberg. Peer reviewer reports are available.

Reprints and permission information is available at http://www.nature.com/reprints

Publisher's note Springer Nature remains neutral with regard to jurisdictional claims in published maps and institutional affiliations.